LETTERS

Towards complete cofactor arrangement in the 3.0 Å resolution structure of photosystem II

Bernhard Loll[1]*†, Jan Kern[2]*, Wolfram Saenger[1], Athina Zouni[2] & Jacek Biesiadka[1]

Oxygenic photosynthesis in plants, algae and cyanobacteria is initiated at photosystem II, a homodimeric multisubunit protein–cofactor complex embedded in the thylakoid membrane[1]. Photosystem II captures sunlight and powers the unique photo-induced oxidation of water to atmospheric oxygen[1,2]. Crystallographic investigations of cyanobacterial photosystem II have provided several medium-resolution structures (3.8 to 3.2 Å)[3–6] that explain the general arrangement of the protein matrix and cofactors, but do not give a full picture of the complex. Here we describe the most complete cyanobacterial photosystem II structure obtained so far, showing locations of and interactions between 20 protein subunits and 77 cofactors per monomer. Assignment of 11 β-carotenes yields insights into electron and energy transfer and photoprotection mechanisms in the reaction centre and antenna subunits. The high number of 14 integrally bound lipids reflects the structural and functional importance of these molecules for flexibility within and assembly of photosystem II. A lipophilic pathway is proposed for the diffusion of secondary plastoquinone that transfers redox equivalents from photosystem II to the photosynthetic chain. The structure provides information about the Mn_4Ca cluster, where oxidation of water takes place. Our study uncovers near-atomic details necessary to understand the processes that convert light to chemical energy.

In photosystem II (PSII), excitation energy is transferred from the antenna system to the reaction centre, where the primary electron donor P680 formed by chlorophyll *a* (Chl*a*) molecules is excited to P680*, followed by release of an electron that travels along the electron transfer chain by means of the pheophytin *a* $Pheo_{D1}$ to the plastoquinone Q_A, forming $P680^{+\bullet}Q_A^{-}$. After two steps of reduction and protonation of the secondary plastoquinone Q_B, the plastoquinol PQH_2 leaves the Q_B site and is replaced by new plastoquinone PQ (ref. 1). Oxidation of water at the Mn_4Ca cluster occurs in four steps (termed S states) in the so-called Kok cycle[2]; at each step the water-oxidizing complex is oxidized to a higher oxidation state, and after the fourth step molecular O_2 is released. The electrons are transferred from the Mn_4Ca cluster through redox-active Tyr_Z to $P680^{+\bullet}$, which is reduced to P680 for another photosynthetic cycle. Our structure of dimeric PSII from *Thermosynechococcus elongatus* shows the location of 35 Chl*a*, 11 β-carotene (Car), two pheophytin (Pheo), two PQ, two haem, bicarbonate, 14 lipid and three *n*-dodecyl-β-D-maltoside (β-DM) detergent molecules, the Mn_4Ca cluster, and one Fe^{2+} and one putative Ca^{2+} ion in each monomer. The cofactor and protein arrangement is shown in Fig. 1 and Supplementary Fig. S1.

Various studies have indicated the influence of lipids on the assembly and function of PSII[7,8], but so far no structural information about lipids bound to PSII is available. We found 14 lipids integrally bound to PSII: four DGDG (digalactosyldiacylglycerol), six MGDG (monogalactosyldiacylglycerol), three SQDG (sulphoquinovosyldiacylglycerol) and one PG (phosphatidyldiacylglycerol) molecule (Fig. 1 and Supplementary Fig. S2). The composition of the lipids is comparable to that of the thylakoid membrane[9]. Hydrophilic lipid headgroups are close to the membrane surface, whereas hydrophobic fatty acid chains are anchored between transmembrane α-helices (TMHs) of different subunits. Negatively charged headgroups of SQDG and PG are exclusively located at the cytoplasmic side (Fig. 1b).

A belt of 11 lipids surrounds the reaction centre, separating it from the antenna and smaller subunits (Fig. 2a). The remaining three lipids and the detergent molecules are located at the monomer–monomer interface. The unusually high lipid content in the PSII complex provides a structural flexibility that might be required for local mobility of subunits and promotes subunit–subunit recognition. At high light intensities, Chl*a* triplet states can be populated and react with molecular oxygen to form singlet oxygen, leading to oxidative damage of proteins. As subunit D1 is most prone to this photodamage, it needs to be continuously replaced by newly synthesized D1 (ref. 10). To facilitate this turnover of D1, a flexible environment, such as that provided by the belt of lipids, might be necessary. A similar 'lubricant' role may be fulfilled by lipid molecules located at the dimerization interface, as observed in other multimeric membrane-intrinsic complexes[11].

The protein environment of Q_A, Q_B and non-haem-Fe^{2+} is described in the Supplementary Discussion and Fig. S3. The Q_B-binding site (Fig. 2b) opens into a large cavity defined by the TMHs of cytochrome *b-559* (PsbE and PsbF), PsbJ, PsbK, TMH-d and TMH-e of D1, and TMH-a of D2 (Fig. 2 and Supplementary Fig. S4). The walls of the cavity are lipophilic as they are coated by phytol chains of P_{D2}, Chl_{D2}, $Pheo_{D2}$, Chl*a*37, Chl*a*44 and Chl*a*46, and by acyl chains of four lipids. In addition, Car11 and Car12 point into the cavity. Fragmented electron density in the cavity is not interpretable and could be due to two or three disordered lipophilic molecules.

The cavity has two openings perpendicular to each other: the larger one (~16 × 16 Å) opens towards the cytoplasmic side and the smaller one (~10 × 20 Å), flanked by TMHs of cytochrome *b-559* and PsbJ, faces the membrane interior (Fig. 2c). On the opposite side of the membrane-facing opening, the Q_B-binding pocket forms an antechamber of the cavity that is filled by the quinone headgroup, while its isoprenoid chain winds along the wall of the cavity. This arrangement suggests that the cavity provides a flexible, lipophilic environment for the diffusion of PQ/PQH_2 through the membrane-facing opening, between the Q_B-binding site in PSII and the plastoquinone pool of the thylakoid membrane (Fig. 2d). Similar lipophilic

[1]Institut für Chemie und Biochemie/Kristallographie, Freie Universität Berlin, Takustrasse 6, D-14195 Berlin, Germany. [2]Institut für Chemie/Max Volmer Laboratorium für Biophysikalische Chemie, Technische Universität Berlin, Straße des 17 Juni 135, D-10623 Berlin, Germany. †Present address: Max-Planck-Institut für Medizinische Forschung, Abteilung für Biomolekulare Mechanismen, D-69120 Heidelberg, Germany.
*These authors contributed equally to this work.

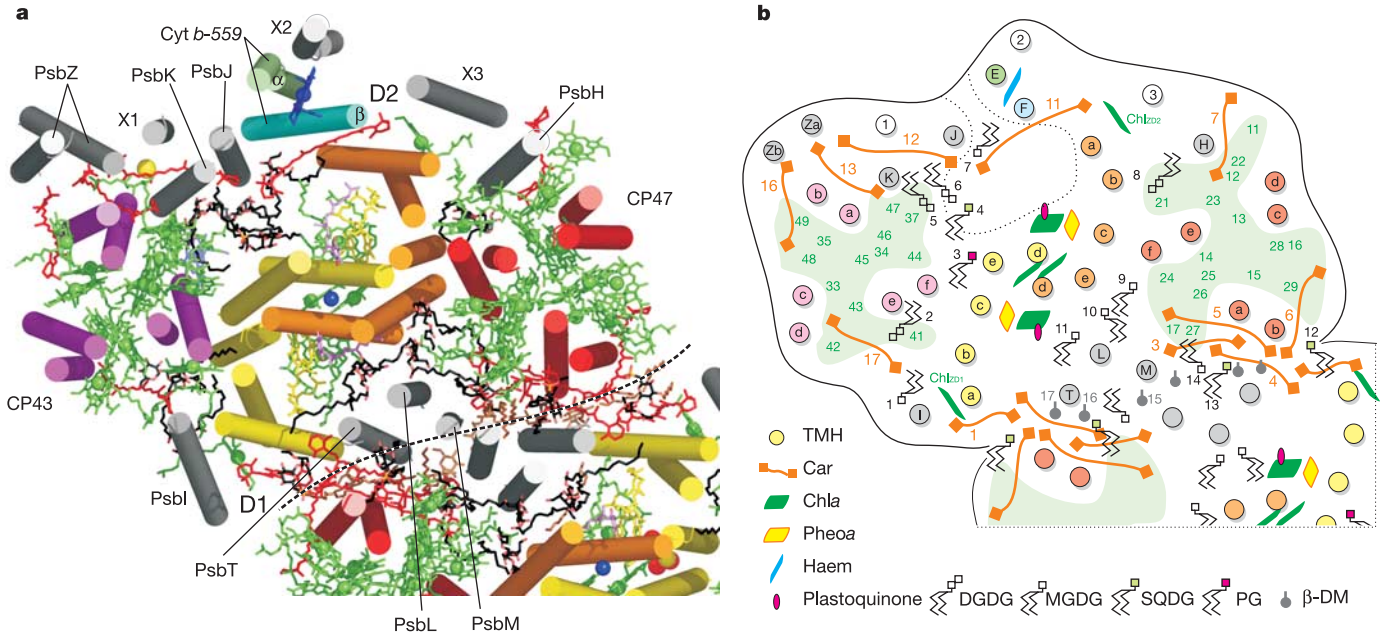

Figure 1 | The PSII monomer from the cytoplasmic side. a, Overall view of the PSII monomer. Transmembrane α-helices are represented as cylinders; other protein elements are omitted for clarity. The main subunits are highlighted as follows: reaction centre subunits D1 (yellow) and D2 (orange), antenna subunits CP43 (magenta) and CP47 (red), and the α- and β-chain of cytochrome *b-559* (green and cyan, respectively). Low molecular mass subunits are coloured grey. Unassigned TMHs are labelled X1–X3. Cofactors are coloured green (Chl*a*), yellow (Pheo), red (Car), blue (haem), violet (quinone), black (lipids) and brown (detergent and unassigned alkyl chains). The non-haem Fe^{2+} (blue) and putative Ca^{2+} (yellow) ions are shown as spheres. Dashed line indicates the monomer–monomer interface. **b**, Schematic representation of the view in **a**, with the same colour code. Lipid and detergent molecules with headgroups pointing 'downwards' or 'upwards' are located at the lumenal or cytoplasmic side, respectively. Green numbers in CP43 and CP47 indicate the positions of antenna Chl*a*. The Q_B diffusion cavity is indicated by a dotted line.

pathways have been proposed for the photosynthetic cytochrome b_6f complex[12,13] and for the respiratory cytochrome bc_1 complex[14]. The alternative exchange pathway for PQ through the larger cytoplasmic opening is less favourable because hydrophobic PQ molecules would have to pass through the cytosol before entering the membrane. It is likely that PsbJ and cytochrome *b-559*, flanking the membrane-facing opening, could regulate PQ diffusion. Indeed, PsbJ has been shown to influence the electron transfer between Q_A, Q_B and the

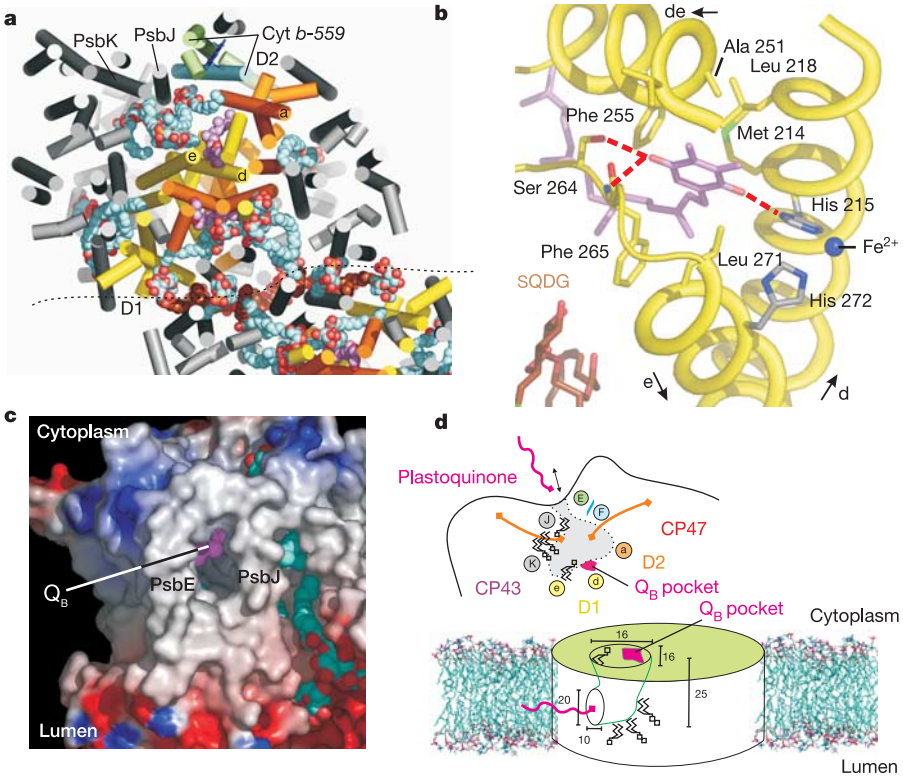

Figure 2 | The plastoquinone diffusion pathway. a, Lipid molecules located in PSII, viewed as in Fig. 1. Lipid, detergent and quinone molecules are shown in space-filling representation, and α-helices of protein subunits are shown as cylinders. Subunits D1 and D2 and cytochrome *b-559* are coloured as in Fig. 1, the remaining α-helices are grey, and lipids are cyan. TMHs forming the wall of the cavity are labelled. **b**, Q_B-binding pocket. The interacting residues of D1 are labelled, arrows indicate orientations of TMH-d and TMH-e, and of the connecting α-helix de. **c**, Electrochemical potential surface of PSII (red, negative; blue, positive; white, neutral), viewed along the membrane plane onto the cavity opening that faces the membrane. The tail of Q_B (violet) is nestled in the cavity. **d**, Schematic views of Q_B diffusion pathway in two orientations. Top, same view as **a**. The positions of TMHs forming the wall of the cavity (circles) and the membrane-facing opening are indicated. Car molecules are orange; lipid molecules are black. Bottom, PSII embedded in the membrane. Positions and approximate dimensions of the two openings of the cavity, as well as the position of the Q_B-binding pocket and lipid molecules, are indicated.

plastoquinone pool in tobacco[15] and, because the haem of cytochrome *b-559* is exposed to the cavity, an influence of the interior of the cavity on the redox properties of cytochrome *b-559* can also be imagined.

The 11 carotenoid molecules were modelled as β-carotene in all-*trans* configuration. Two carotenoids are bound to the D1 and D2 subunits (Fig. 3), three are at CP43 and five at CP47 (Fig. 1). Car12 is nestled between subunits PsbJ, PsbK, PsbZ and X1. The carotenoids are distributed uniformly at the periphery of PSII except for Car3, Car4, Car5 and Car6, which are clustered at the monomer–monomer interface. This contrasts with the arrangement of seven Car molecules in previous work[5] (Supplementary Discussion). In the reaction centre, Car_{D2} (Car11) is nearly parallel to the membrane plane and located close to cytochrome *b-559*, as shown in previous models[5,6]. Its counterpart Car_{D1} (Car1) is oriented roughly perpendicular to the membrane plane, the isoprenoid moiety being parallel to TMH-a of D1 (Fig. 3a and Supplementary Fig. S5). The presence of two differently oriented and therefore spectroscopically distinct Car molecules has been shown for spinach PSII (ref. 16), where Car_{D1} corresponds to Car_{489} and Car_{D2} to Car_{507}.

Because Car_{D1} does not bridge between $Chlz_{D1}$ and other cofactors of the electron transfer chain (Fig. 3b), it is unlikely that Car_{D1} participates in electron transfer reactions. Its position is rather optimized for transfer and/or quenching of $Chlz_{D1}$ triplet states and quenching of singlet oxygen that could be produced by $^3P680$ (ref. 17). By contrast, the position of Car_{D2} seems to be less efficient for quenching of triplet states, but is in keeping with a role as a 'molecular wire' in putative secondary electron transfer when the Mn_4Ca cluster is not functional or is absent[17]. This idea is supported by calculations of maximal electron transfer rates, showing that secondary electron transfer reactions will predominantly occur on the D2 side (Supplementary Table S4).

Most of the Car molecules located in the antenna subunits are in van der Waals contact with Chl*a* molecules, thereby allowing transfer of excitation energy from Car to Chl*a*, as well as protection of PSII from destructive triplet states of Chl*a* by means of rapid triplet–triplet transfer. However, not all Chl*a* molecules are located close to a Car molecule. As coupled Chl*a* molecules of the antenna might act as excitation energy sinks, with a longer lifetime of the excited state and hence higher probability of triplet formation, sufficient protection from triplet states could be achieved if these groups are connected to at least one Car molecule. Strongest coupled Chl*a* groups in CP47 (Chl*a*11, Chl*a*12, Chl*a*13 and Chl*a*14, Chl*a*17, Chl*a*25, Chl*a*26, Chl*a*27) have a Car molecule at van der Waals contact, whereas corresponding groups in CP43 (Chl*a*34, Chl*a*46 and Chl*a*45, Chl*a*47) are more distant from any Car, indicating lower triplet quenching efficiency. A cluster of four Car molecules (Car3, Car4, Car5 and Car6) is located at the monomer–monomer interface, close to a coupled group of five Chl*a* molecules in CP47 (Fig. 1 and Supplementary Fig. S6). Three of the clustered Car molecules are at van der Waals distance to each other, forming a coupled Car multimer, which could broaden the absorption spectrum of the antenna system.

The shape of the electron density of the Mn_4Ca cluster can be best approximated by four Mn ions arranged as a 'hook' (Fig. 4a) resembling a Y-shaped structure[3,6]. The Mn ions are numbered Mn1 to Mn4, starting from the highest electron density at the bend of the 'hook'. The Mn–Mn distances could not be derived directly at 3.0 Å resolution and thus were crystallographically refined with the aid of restraints obtained from EXAFS studies (Supplementary Methods). Mn1–Mn2 and Mn2–Mn3 are 2.7 Å apart and probably connected by di-μ-oxo bridges, whereas Mn1–Mn3 and Mn3–Mn4 are at 3.3 Å, suggesting mono-μ-oxo bridges (Fig. 4b). This arrangement is compatible with the '3 + 1' models suggested for the Mn cations[18]. The position of Ca^{2+} between the Mn and Tyr_Z is supported by spherical anomalous difference electron density (Supplementary Fig. S7). Ca^{2+} forming the vertex of a trigonal pyramid is equidistant (~3.4 Å) to Mn1, Mn2 and Mn3.

The interpretation of the Mn_4Ca structure and coordination must account for likely radiation damage of the cluster during X-ray data collection. EXAFS studies of PSII crystals and solutions indicated that Mn^{3+} and Mn^{4+} ions of the Mn_4Ca cluster are rapidly reduced by X-ray generated radicals to Mn^{2+} (ref. 19). This reduction is probably associated with structural changes caused by the disruption of μ-oxo bridges and Mn–ligand interactions and may lead to disorder, as indicated by uneven distribution of electron density in the cluster (Supplementary Fig. S7).

The two short and two long Mn–Mn interactions and the three equal Mn–Ca^{2+} interactions differ from the numbers of such interactions derived from EXAFS studies[20]. This discrepancy could be caused by the still low resolution of the diffraction data and by possible radiation damage. In particular, the positions of Ca^{2+} and Mn4 are less well defined in the electron density, leading to higher coordinate errors for these atoms. The proposed coordination of Mn and Ca^{2+} is shown in Fig. 4b. The residues of the second coordination

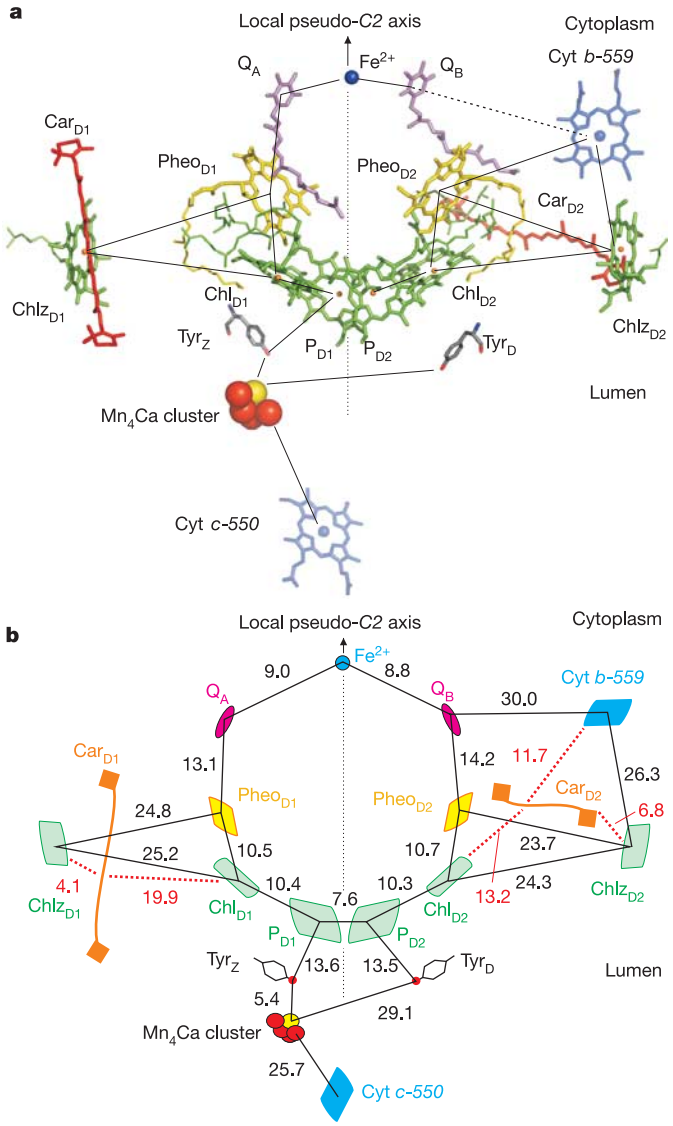

Figure 3 | Redox-active cofactors and electron transfer chain. a, View along the membrane plane. The cofactors of the electron transfer chain (P_{D1}/P_{D2}, Chl_{D1}/Chl_{D2}, $Pheo_{D1}/Pheo_{D2}$, Q_A/Q_B) are related by the pseudo-*C2* axis (arrow). Fe^{2+} (blue), Mn (red) and Ca^{2+} (yellow) ions are shown as spheres. **b**, Schematic representation of the view in **a**. Selected distances (in angstroms) are drawn between cofactor centres (black lines) and edges of π systems (red dotted lines).

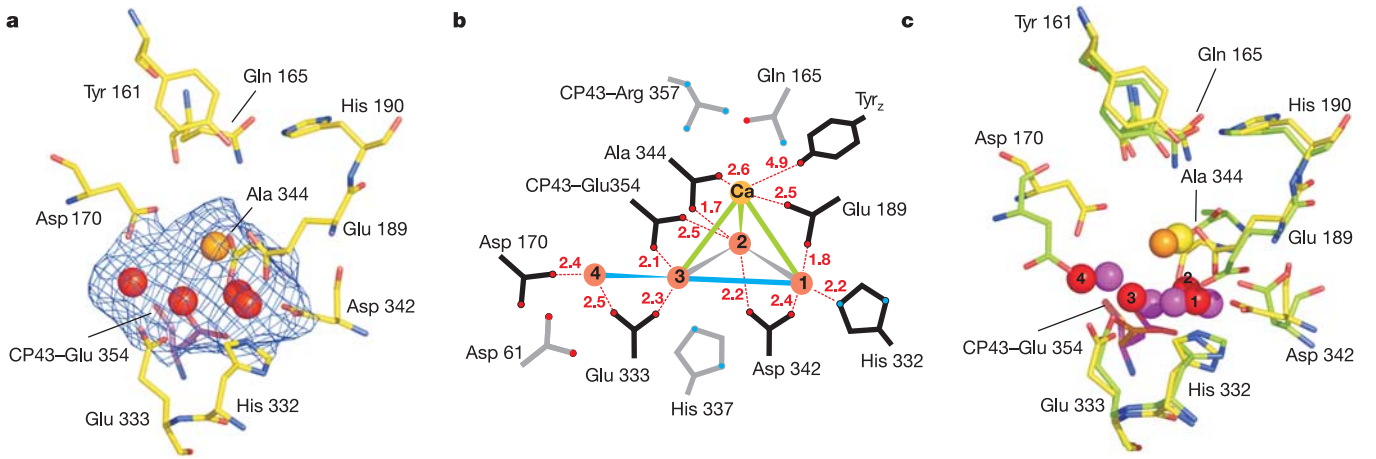

Figure 4 | Oxygen-evolving centre. a, Electron density of the Mn_4Ca cluster, viewed similarly to Fig. 3a. Surrounding amino acids of D1 (yellow) and CP43 (magenta) are indicated; Mn is red and Ca^{2+} is orange. The $2F_o - F_c$ map is contoured at the 1.2σ level. **b**, Schematic view of the Mn_4Ca cluster. Distances between Mn (red) and Ca^{2+} (orange) are indicated by the connecting lines (grey, 2.7 Å; blue, 3.3 Å, green, 3.4 Å). Amino acids of the first coordination sphere are black; those of the second sphere are grey; distances are given in angstroms. **c**, Superposition of the current Mn_4Ca structure (coloured as in **a**) with that of ref. 5 (D1 in green, CP43 in orange, Mn in violet and Ca^{2+} in yellow, respectively).

sphere (Fig. 4b, grey), even though they are not close enough to coordinate the Mn_4Ca cluster directly in the oxidation states present in the crystals, might be suitable for interaction through water molecules or may provide ligation in different redox states of the Mn_4Ca cluster.

Although the limited resolution does not allow a definite decision about rotamers of ligating side chains, five carboxylates are in positions that could act as bidentate ligands bridging different cations. The combination of bidentate ligands and mono- or di-μ-oxo bridges could enhance the stability of the cation arrangement and facilitate rearrangement of μ-oxo bridges during the S-state cycle. Mutational studies of ligating residues[21,22] found that, except for Glu 333 and Asp 342 of D1, replacement of a ligating group with a non-ligating group still leads to a (partially) functional cluster. Our structure shows that in most cases a second ligating group is present, which could hold the cations in place even when the exchanged residue cannot coordinate them.

Glu 189 and Ala 344 in D1 are identified as possible ligands for Ca^{2+}, with the former also ligating Mn1 and the latter Mn2, in contrast to previous findings[5]. Taking into account the positional error of Ca^{2+} and results from Fourier transform infrared (FTIR) spectroscopy indicating that Ala 344 of D1 should ligate Mn (ref. 23) but not Ca^{2+} (ref. 24), it is likely that Ca^{2+} is coordinated only by Glu 189 of D1. Mn4, which is coordinated by Asp 170 and Glu 333 of D1 and represents the first Mn ion bound to the high-affinity binding site during assembly of the cluster[22,25], seems to be more distinct from the other three Mn ions. Our electron density suggests that Mn4 is most prone to radiation damage and subsequent disorder.

Our structure of the Mn_4Ca cluster differs considerably from the postulated cubane-like model[5] because the Mn–Mn distances in the pyramid formed by three Mn and Ca^{2+} are not equal and the pyramid is connected asymmetrically to Mn4 (Fig. 4c; for a detailed comparison of both structures, see Supplementary Discussion and Fig. S8). Even though the same coordinating residues have been proposed[5], none of them was modelled as bridging two metal ions, leading to a lower saturation of the metal coordination spheres. Consequently, the restraints for possible μ-oxo-bridging are altered, resulting in a different architecture of the whole oxygen-evolving complex and providing new implications for the mechanism of water oxidation.

Combining the structure with results from FTIR studies[23,26,27] and assuming an oxidation state distribution of $Mn(III)_2(IV)_2$ for the S_1 state of the Kok cycle[28,29], we can suggest localization of oxidation states on individual metal ions of the cluster. Mn1 and Mn3 can attain either oxidation state III or oxidation state IV in the S_1 state. Mn4, which is ligated by Asp 170, is not oxidized during S_0–S_1–S_2–S_3 transitions[26] and is therefore probably present as Mn(IV), whereas Mn2, which is ligated by the carboxy-terminal carboxylate of Ala 344, changes from Mn(III) to Mn(IV) in the S_1–S_2 transition[23] and can be considered as the site of first oxidation in the catalytic cycle of water splitting.

METHODS

Dimeric PSII from *T. elongatus* was purified, characterized and crystallized as described[30]. X-ray diffraction data were collected at the European Synchrotron Radiation Facility (ESRF, Grenoble, France). The crystal structure of PSII was determined to 3.0 Å resolution and refined to R and R_{free} factors of 0.24 and 0.29, respectively (Supplementary Methods and Tables S1 and S2).

Received 1 July; accepted 13 September 2005.

1. Ke, B. *Photosynthesis—Photobiochemistry and Photobiophysics* (Kluwer Academic, Dordrecht, 2001).
2. Kok, B., Forbush, B. & McGloin, M. Cooperation of charges in photosynthetic evolution: I. A linear four step mechanism. *Photochem. Photobiol.* **11**, 457–475 (1970).
3. Zouni, A. *et al.* Crystal structure of photosystem II from *Synechococcus elongatus* at 3.8 Å resolution. *Nature* **409**, 739–743 (2001).
4. Kamiya, N. & Shen, J. R. Crystal structure of oxygen-evolving photosystem II from *Thermosynechococcus vulcanus* at 3.7-Å resolution. *Proc. Natl Acad. Sci. USA* **100**, 98–103 (2003).
5. Ferreira, K. N., Iverson, T. M., Maghlaoui, K., Barber, J. & Iwata, S. Architecture of the photosynthetic oxygen-evolving center. *Science* **303**, 1831–1838 (2004).
6. Biesiadka, J., Loll, B., Kern, J., Irrgang, K.-D. & Zouni, A. Crystal structure of cyanobacterial photosystem II at 3.2 Å resolution: a closer look at the Mn-cluster. *Phys. Chem. Chem. Phys.* **6**, 4733–4736 (2004).
7. Gombos, Z. *et al.* Phosphatidylglycerol requirement for the function of electron acceptor plastoquinone Q_B in the photosystem II reaction center. *Biochemistry* **41**, 3796–3802 (2002).
8. Steffen, R., Kelly, A. A., Huyer, J., Dörmann, P. & Renger, G. Investigations on the reaction pattern of photosystem II in leaves from *Arabidopsis thaliana* wild type plants and mutants with genetically modified lipid content. *Biochemistry* **44**, 3134–3142 (2005).
9. Wada, H. & Murata, N. in *Lipids in Photosynthesis: Structure, Function and Genetics* (ed. Murata, N.) 65–81 (Kluwer Academic, Dordrecht, 1998).
10. Baena-Gonzalez, E. & Aro, E. M. Biogenesis, assembly and turnover of photosystem II units. *Phil. Trans. R. Soc. Lond. B* **357**, 1451–1459 (2002).
11. Palsdottir, H. & Hunte, C. Lipids in membrane protein structures. *Biochim. Biophys. Acta* **1666**, 2–18 (2004).
12. Stroebel, D., Choquet, Y., Popot, J. L. & Picot, D. An atypical haem in the cytochrome b_6f complex. *Nature* **426**, 413–418 (2003).

13. Kurisu, G., Zhang, H., Smith, J. L. & Cramer, W. A. Structure of the cytochrome b_6f complex of oxygenic photosynthesis: tuning the cavity. *Science* **302,** 1009–1014 (2003).
14. Lange, C., Nett, J. H., Trumpower, B. L. & Hunte, C. Specific roles of protein–phospholipid interactions in the yeast cytochrome bc_1 complex structure. *EMBO J.* **20,** 6591–6600 (2001).
15. Ohad, I., Dal Bosco, C., Herrmann, R. G. & Meurer, J. Photosystem II proteins PsbL and PsbJ regulate electron flow to the plastoquinone pool. *Biochemistry* **43,** 2297–2308 (2004).
16. Kwa, S. L. S., Newell, W. R., van Grondelle, R. & Dekker, J. P. The reaction center of Photsystem II studied with polarized fluorescence spectroscopy. *Biochim. Biophys. Acta* **1099,** 193–202 (1992).
17. Telfer, A. What is β-carotene doing in the photosystem II reaction centre? *Phil. Trans. R. Soc. Lond. B* **357,** 1431–1440 (2002).
18. Peloquin, J. M. & Britt, R. D. EPR/ENDOR characterization of the physical and electronic structure of the OEC Mn cluster. *Biochim. Biophys. Acta* **1503,** 96–111 (2001).
19. Yano, J. *et al.* X-ray damage to the Mn_4Ca complex in single-crystals of photosystem II: a case study for metallo-protein X-ray crystallography. *Proc. Natl Acad. Sci. USA* **102,** 12047–12052 (2005).
20. Sauer, K., Yano, J. & Yachandra, V. K. X-ray spectroscopy of the Mn_4Ca cluster in the water-oxidation complex of photosystem II. *Photosynth. Res.* **85,** 73–86 (2005).
21. Diner, B. A. Amino acid residues involved in the coordination and assembly of the manganese cluster of photosystem II. Proton-coupled electron transport of the redox-active tyrosines and its relationship to water oxidation. *Biochim. Biophys. Acta* **1503,** 147–163 (2001).
22. Debus, R. J. Amino acid residues that modulate the properties of tyrosine Y(Z) and the manganese cluster in the water oxidizing complex of photosystem II. *Biochim. Biophys. Acta* **1503,** 164–186 (2001).
23. Kimura, Y., Mizusawa, N., Yamanari, T., Ishii, A. & Ono, T. A. Structural changes of D1 C-terminal α-carboxylate during S-state cycling in photosynthetic oxygen evolution. *J. Biol. Chem.* **280,** 2078–2083 (2005).
24. Strickler, M. A., Walker, L. M., Hillier, W. & Debus, R. J. Evidence from biosynthetically incorporated strontium and FTIR difference spectroscopy that the C-terminus of the D1 polypeptide of photosystem II does not ligate calcium. *Biochemistry* **44,** 8571–8577 (2005).
25. Campbell, K. D. *et al.* Dual-mode EPR detects the initial intermediate in photoassembly of the photosystem II Mn cluster: the influence of amino acid residue 170 of the D1 polypeptide on Mn coordination. *J. Am. Chem. Soc.* **122,** 3754–3761 (2000).
26. Debus, R. J., Strickler, M. A., Walker, L. M. & Hillier, W. No evidence from FTIR difference spectroscopy that aspartate-170 of the D1 polypeptide ligates a manganese ion that undergoes oxidation during the S_0 to S_1, S_1 to S_2, or S_2 to S_3 transitions in photosystem II. *Biochemistry* **44,** 1367–1374 (2005).
27. Kimura, Y., Ishii, A., Yamanari, T. & Ono, T. A. Water-sensitive low-frequency vibrations of reaction intermediates during S-state cycling in photosynthetic water oxidation. *Biochemistry* **44,** 7613–7622 (2005).
28. Roelofs, T. A. *et al.* Oxidation states of the manganese cluster during the flash-induced S-state cycle of the photosynthetic oxygen-evolving complex. *Proc. Natl Acad. Sci. USA* **93,** 3335–3340 (1996).
29. Dau, H., Iuzzolino, L. & Dittmer, J. The tetra-manganese complex of photosystem II during its redox cycle—X-ray absorption results and mechanistic implications. *Biochim. Biophys. Acta* **1503,** 24–39 (2001).
30. Kern, J. *et al.* Purification, characterisation and crystallisation of photosystem II from *Thermosynechococcus elongatus* cultivated in a new type of photobioreactor. *Biochim. Biophys. Acta* **1706,** 147–157 (2005).

Supplementary Information is linked to the online version of the paper at www.nature.com/nature.

Acknowledgements We thank D. DiFiore and C. Lüneberg for technical assistance; K.-D. Irrgang, H. Lokstein, J. Messinger, F. Müh, T. Renger, E. Schlodder and J. Yano for discussions; and R. Clarke, G. Renger, K. Sauer and V. Yachandra for critically reading the manuscript. Beam time and support at the ESRF, SLS, BESSY and DESY are gratefully acknowledged. We thank Deutsche Forschungsgemeinschaft and Fonds der Chemischen Industrie for support.

Author Information Atomic coordinates have been deposited in the Protein Data Bank under the accession number 2AXT. Reprints and permissions information is available at npg.nature.com/reprintsandpermissions. The authors declare no competing financial interests. Correspondence and requests for materials should be addressed to W.S. (saenger@chemie.fu-berlin.de) and A.Z. (zouni@phosis1.chem.tu-berlin.de).